ISSN: 1410-8917
e-ISSN: 2597-9914

Jurnal Kimia Sains dan Aplikasi 25 (10) (2022): 382–393

Jurnal Kimia Sains dan Aplikasi
Journal of Scientific and Applied Chemistry

Journal homepage: http://ejournal.undip.ac.id/index.php/ksa

Screening of Secondary Metabolite Compounds of Gorontalo Traditional Medicinal Plants Using the In Silico Method as a Candidate for SARS-CoV-2 Antiviral

Yuszda K. Salimi [a], La Ode Aman [a], Zaenul Wathoni [a,*], Netty Ino Ischak [a], Akram La Kilo [a], La Alio

[a] Department of Chemistry, Faculty of Sciences and Mathematics, Universitas Negeri Gorontalo, Gorontalo, Indonesia

* Corresponding author: zaenal_s1kimia2018@mahasiswa.ung.ac.id

https://doi.org/10.14710/jksa.25.10.382-393

Article Info

Article history:

Received: 6th October 2022
Revised: 13th December 2022
Accepted: 24th December 2022
Online: 25th December 2022

Keywords:
Antivirals; SARS-CoV-2; molecular docking; molecular dynamics; COVID-19

Abstract

COVID-19 is a disease that caused a prolonged pandemic in many countries caused by the SARS-CoV-2 virus. This study aims to identify the antiviral potential of secondary metabolites in Gorontalo traditional medicinal plants, which are believed to have the ability to inhibit the main protease protein of this virus. The methods used in this research were molecular docking and molecular dynamic. The main protease proteins for SARS-CoV-2 used based on the homology modeling results were 3V3M and 7TE0. The results of the active compounds in the paxlovid drug were also compared to obtain accurate data comparisons. The validation of the docking method on the 3V3M protein using the natural ligand 0EN revealed an RMSD of 0.75 Å. The RMSD value for validating the 7TE0 protein and natural ligand 4WI was 1.65 Å. The best molecular docking results were obtained using physalin F with a binding affinity of -10.3 kcal/mol for the 3V3M protein and physalin J with a binding affinity of -8.9 kcal/mol for the 7TE0 protein. The outcomes of the molecular dynamic method on the best complexes were determined by examining the value of changes in system energy, changes in system temperature, changes in system pressure, RMSD, RMSF, and bond-free energy (ΔG) of the complex. The standard 0EN ligand had a ΔG of -26.53 kcal/mol, while the standard 4WI ligand had a ΔG of -47.16 kcal/mol. The ΔG of the 3V3M-physalin F and 3V3M-physalin J complexes were respectively -28.22 kcal/mol and -26.62 kcal/mol. The ΔG of the 7TE0-Vitexin 2”-O-gallate and 7TE0-physalin J complexes were found to be -28.08 kcal/mol and -26.62 kcal/mol, respectively. The ΔG produced in paxlovid with complexes 3V3M and 7TE0 was -19.38 kcal/mol and -25.44 kcal/mol, respectively. Physalin F, physalin J, and Vitexin 2”-O-gallate have great potential to become SARS-CoV-2 inhibitor agents. However, in terms of structural stability and binding-active residues, these three compounds do not outperform the active substance in paxlovid.

1. Introduction

COVID-19 is an infection brought on by the highly contagious pathogen severe acute respiratory syndrome coronavirus 2 (SARS-CoV-2), which has caused a worldwide pandemic. According to genome analysis, bats are the primary reservoir of infection for this disease. Although widespread human-to-human transmission has been proven, the exact method by which the pathogen was transmitted from bats to humans is unknown [1]. COVID-19 has spread to many nations, with the United States, United Kingdom, Germany, Denmark, France, Canada, Japan, India, Sweden, and Brazil registering the highest number of confirmed infections [2]. In the human body, SARS-CoV-2 RNA found in infected samples can cause lung

transmission by binding to angiotensin-converting enzyme-2 (ACE-2) from alveolar epithelial cells [3].

Initial infection with SARS-CoV-2 occurs through inhalation of air that passes through the throat, bronchioles, and alveoli. The alveoli and trachea are respiratory system organs responsible for gas exchange. Mucus in the trachea, bronchi, and bronchioles filter microorganisms entering the respiratory system of humans. Inhaling the SARS-CoV-2 virus causes the bronchioles and alveoli to become inflamed, leading to acute inflammatory disease. The inability to detect the threat and the incapacity of the immune system to repair the damage caused by the SARS-CoV-2 virus have led to a deterioration of the diseased body. The SARS-CoV-2 virus will continue to multiply if additional treatments are not administered to inhibit its replication [4].

The COVID-19 pandemic caused many changes to the order of life in the world community. The economic, social, cultural, and even employment sectors have experienced a very significant impact due to this pandemic. Restrictions on activities are implemented in various nations to slow the spread. The new habit of working from home is also a tremendous change that has an impact on the economy, society, and even in terms of technology which requires the entire world's population to adapt to prevent the spread of COVID-19 [5]. The health sector has been the sector most severely affected. The inability to supply nutrient-rich food sources and the lack of access to healthcare in some countries have both led to an increase in mortality regardless of age [6].

Play protease (Mpro), also known as 3C-like protease (3CLpro), is a part of the protein structure that is included in the non-structural protein category. Therefore, the main protease is also called nsp5. The main protease has more than 11 cleavage sites. Inhibition of this enzyme activity can cause inhibition of the viral replication process [7] as shown in Figure 1. Mpro is a 33.8-kDa cysteine protease that mediates the maturation of functional polypeptides that are directly involved in the replication process of viral transcription. This enzyme is essential in the survival of the SARS-CoV-2 virus by mediating transcription and viral protein replication. The role of the main protease as a virus replication agent is what underlies many researchers to study and find inhibitors of the replication process and make them targets in designing antivirals/antiviruses for SARS-CoV-2 [8].

Figure 1. Structure of the main protease of SARS-CoV-2

All countries require antiviral drugs capable of inhibiting viral replication in infected human bodies to prevent the SARS-CoV-2 virus from spreading to other cells [9]. Antiviral production is growing over time. Active compounds considered to affect the healing of COVID-19 patients have traditionally been tested to determine the level of inhibitory ability of these compounds against the main protease of the SARS-CoV-2 virus.

In more detail, the mechanism of antiviral inhibition of the main protease SARS-CoV-2 can be seen in Figure 2 and Figure 3. Generally, SARS-CoV-2 infection begins with the attachment of the virus to the cell membrane of the human body. This attachment is characterized by an interaction between the S protein in the virus and the ACE2 receptor. A membrane fusion occurs once the virus has entered the cell, releasing it into the cytoplasm and translating into the polyproteins pp1a and 1ab. Moreover, antiviral compounds administered orally into the human body inhibit the principal protease of SARS-CoV-2 during the proteolysis stage, as shown in Figure 2, step number 3. Thus, the replication and transcription processes of the SARS-CoV-2 virus can be halted [10].

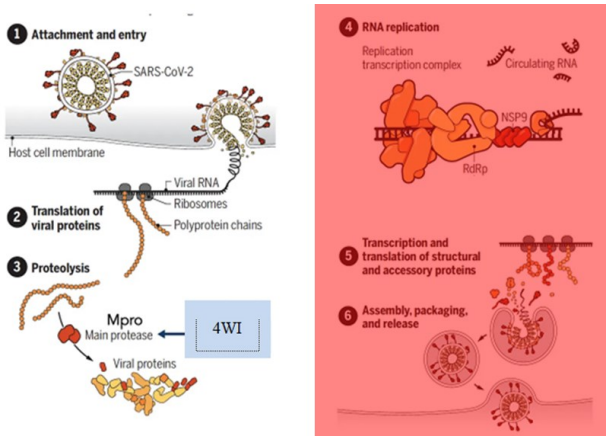

Figure 2. Mechanism of inhibition of the main protease by antivirals [10]

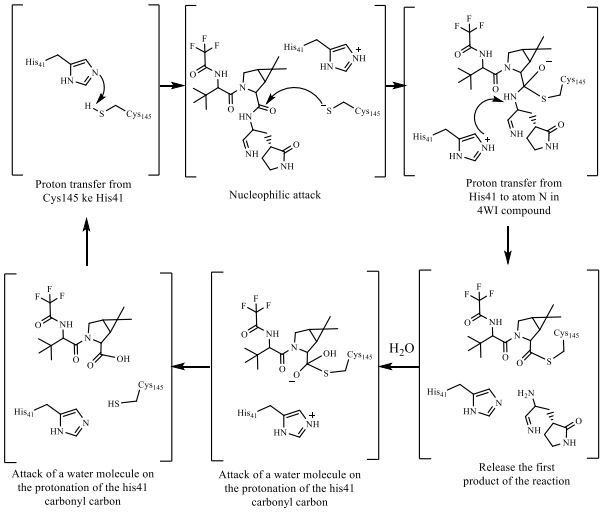

Figure 3. Mechanism of antiviral inhibition of active amino acids (Cys145 and His41) in the main protease of SARS-CoV-2 [11]

Paxlovid whose structure is presented in Figure 4 is an oral antiviral drug that reduces the ability of SARS-CoV-2 to reproduce in the body. The active substance PF-07321332 blocks the activity of enzymes required by viruses to replicate [12]. Paxlovid reduces mortality and hospitalization rates among COVID-19 patients. COVID-19 patients can safely use the drug as a therapeutic agent since it has no side effects [13]. Therefore, this study used the active compound in paxlovid as a comparison.

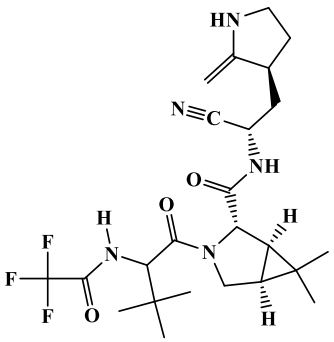

Figure 4. Structure of paxlovid antiviral compound

Indonesia can be explored for potential COVID-19 drug candidates due to its abundance of plant species and the widespread use of these plants in traditional medicine [14]. Gorontalo is one of the regions with a relatively high prevalence of distribution and utilization of traditional medicinal plants. Traditional medicines are concoctions derived from natural ingredients with minimal processing but have a genuine therapeutic effect and are passed down from generation to generation [15]. Traditional medicinal plants in Gorontalo have many types and uses. Several types of plants that are commonly used in traditional medicine, such as shallots (*Allium cepa* L.), garlic (*Allium sativum*), green chiretta (*Andrographis paniculata*), yellow-fruit moonseed (*Arcangelisia flava* L.), papaya (Carica papaya), *Centella asiatica*, cinnamon (*Cinnamomum zeylanicum*), kaffir lime (*Citrus hystrix*), coriander (*Coriandrum sativum*), turmeric (*Curcuma longa*), asthma weed (*Euphorbia hirta*), physic nut (*Jatropha curcas*), plantain (*Musa balbisiana*), cutleaf groundcherry (*Physalis angulata* L.), caraway seed (*Trachyspermum roxburghianum*), blue porterweed (*Stachytarpheta jamaicensis*), kejibeling (*Strobilanthes crispa*), clove (*Syzygium aromaticum*), Indian almond (*Terminalia catappa*), ginger (*Zingiber officinale*), white turmeric (*Curcuma zedoaria*) and Javanese turmeric (*Curcuma xanthorrhiza*). Traditional medicinal plants that treat fever, headaches, shortness of breath, coughs, body aches, and stomach aches may potentially inhibit SARS-CoV-2 replication [14, 16]. This is consistent with the symptoms in patients exposed to this virus.

The 380 secondary metabolites in Gorontalo traditional medicinal plants were thoroughly selected based on the stored database on the KNApSAcK-3D website (http://knapsack3d.sakura.ne.jp/). The website is a three-dimensional structure database maintained by the Maebashi Institute of Technology and the Nara Institute of Science and Technology. In this study, all of these compounds were evaluated. In order to determine SARS-CoV-2 antiviral candidates from active compounds found in traditional Gorontalo medicinal plants, a technique that can provide accurate data on ligand binding as the principal protease inhibitor agent for SARS-CoV-2 is required. This research employed molecular docking and molecular dynamic methods.

2. Methodology

2.1. Tools and Materials

The tools used in this research were a computer HP L1950 12-core CPU with Intel® Xenon® CPU X5675 @ 3.07GHz. Molecular docking and molecular dynamic simulations were supported with the help of several applications such as AutoDock Tools version 1.5.7 [17], Autodock Vina version 1.2.0 [18], Discovery studio visualizer version 21.1.0.20298 [19], Notepad++ version 8.4.7 [20], Perl IDE version 5.14.21 [21], Open Babel version 2.3.1 [22], Pymol version 4.60 [23], Gromacs version 2022.1 [24], and xmgrace version 5.1.19 [25]. The materials used in this study were taken from several websites. The amino acid sequence of the main protease of SARS-CoV-2 can be accessed at the China National Center for Bioinformation 2019 Novel Coronavirus Resource (CNCB 2019nCoV) [26] Wuhan variation with access code MN908947.3 and omicron variation with code OM532067.1 [2]. The 380 test ligands were downloaded on the KNApSAcK-3D page (http://knapsack3d.sakura.ne.jp/). The 380 test ligands derived from traditional Gorontalo medicinal plants can be seen in Table S1. In addition to the active substance PF-07321332 in the drug paxlovid, which was also tested in this simulation, the three-dimensional structure of the active substance paxlovid was downloaded on the Pubchem compound server.

2.2. Homology modeling

Sequence data obtained were subjected to homology modeling to obtain a template structure used in the docking process. Homology modeling was performed using the I-TASSER website (https://zhanggroup.org/I-TASSER/). The results of homology modeling were ten templates with different C-scores.

2.3. Docking method validation

The docking procedure was initially validated before docking the test ligands to assess its probability of success. Ligands and proteins were prepared using AutoDock Tools version 1.5.7. The preparation stage included removing water molecules, adding hydrogen atoms, adding charges, making a grid, and docking parameters. The grid box used was different for each test protein.

2.4. Docking of test ligands

The test ligands were prepared before entering the molecular docking process. The preparation stage was conducted to obtain a more stable ligand structure with lower energy. The stage of test ligand preparation included geometry optimization and energy minimization utilizing the Chem 3D Professional software and the MM2 forcefield. The ligand file format

was then changed to the formal .pdbqt using the Open Babel GUI software.

After the preparation, ligand testing was performed by docking the molecule to the protein. The docking process was carried out using the Autodock Vina program, which is run with the Padre script from the Perl IDE (https://padre.perlide.org/) to facilitate the docking process in large numbers continuously. The script was downloaded and installed on the employed computer. The grid box used in this simulation was adjusted to the results of the previous docking validation so that the test ligand bound to the protein's active site.

2.5. Molecular dynamic simulation

Molecular dynamic simulation is a method of calculating the evolution of systems and the movement of particles within a certain time interval. This method can show the stability of the complex between the protein and the ligand as a result of the previous molecular docking. This process was performed using the Gromacs program version 2022.1 [24]. This simulation included the creation of protein and ligand topologies, solvency and neutralization, energy minimization and equilibration, MD production, and MMGBSA analysis.

3. Results and Discussion

3.1. Homology Modeling

I-TASSER webserver homology modeling of the primary protease sequence previously obtained on the 2019nCoV CNCB server with the codes MN908947.3 for the Wuhan variant and OM532067.1 for the omicron variant. The homology modeling results were ten templates selected by comparing the highest C-score. The template with the highest C-score on the Wuhan variation was downloaded with the PDB code 3V3M, while the omicron variation was downloaded with the code 7TE0 [27] as shown in Figure 5.

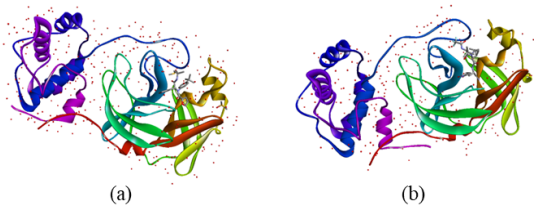

Figure 5. SARS-CoV-2 protein template a) Wuhan (3V3M), b) omicron (7TE0)

3.2. Docking Method Validation

Before validating the docking method, protein and ligand preparation must be performed for optimal docking results. The presence of water molecules in the protein structure can interfere with the binding process between ligands and proteins, resulting in suboptimal docking [28]. The addition of hydrogen atoms also needs to be done so that the hydrogen bonds formed are easier to observe [29]. Partial charges on the ligand and protein are added, respectively, Gasteiger and Kollman charge. Figures 6 and 7 show illustrations of natural proteins and ligands.

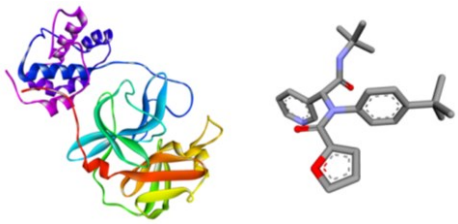

Figure 6. 3V3M protein and natural ligand 0EN

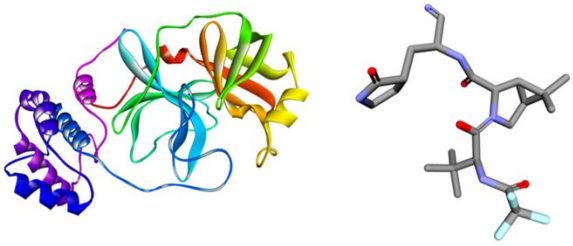

Figure 7. 7TE0 protein and natural ligand 4WI

The natural ligand docking method was validated using AutoDock Tools. The grid box used as a ligand binding area for the protein's active site differs in the 3V3M and 7TE0 proteins. The grid size of the 3V3M protein has center x = 22.99, y = -27.239, z = -3.350 with size xyz respectively 12-12-10. The grid box size utilized for the 7TE0 protein was centered at x = -10.632, y = -14.534, and z = -17.396, with an xyz size of 12-12-8. Spacing on the grid box of both proteins was set at 1 Å.

Table 1. Natural ligand molecular docking results

Ligand	Run	Binding energy (kcal/mol)	Cluster	RMSD (Å)
0EN	9	-7.20	7	0.75
4WI	9	-6.12	3	1.65

The results of the docking of natural proteins and ligands are shown in Table 1. The docking method is valid and can be used if the resulting RMSD value is ≤ 2 Å [30]. In Figure 8, the overlay results on the ligand are shown in red (before the docking process) and green (after the docking process). The overlap shows the ligand's position's minimal deviation after docking. The overlap is tighter the lower the RMSD value.

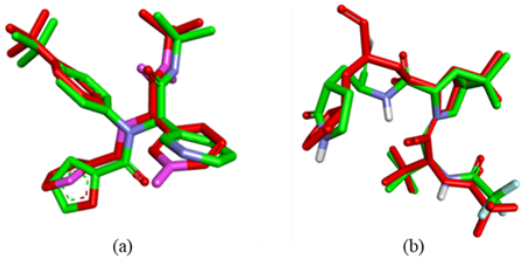

Figure 8. Docking results overlay a) 0EN, b) 4WI

The interaction of amino acid residues in the 3V3M-0EN complex is shown in Figure 9. Many hydrogen bonds are formed in the amino acids Gly143, Cys145, Glu166, Ser144, and Asn142. The formed bonds have different distances. In addition to hydrogen bonds, pi-sulfur bonds are formed on the amino acids Met49 and Cys145, and there are hydrophobic bonds on the amino acid His41. In the 7TE0-4WI complex, hydrogen bonds are created in the amino acids Cys145, Glu166, Gln192,

and Glu166. Halogen bonds are also formed in this complex at the amino acids Glu166, Arg188, and Thr190. Hydrophobic interactions occur at the amino acids His41, Cys145, and His163. Complete interactions in the 3V3M and 7TE0 complexes can be seen in Tables 2 and 3.

Table 2. 0EN ligand interaction on docked 3V3M protein

Category	Interaction	Bond distance (Å)	bond type
Hydrogen bond	gly143	2.42503	Conventional Hydrogen Bonds
	Cys145	2.97913	Conventional Hydrogen Bonds
	Glu166	2.11781	Conventional Hydrogen Bonds
	Ser144	2.46627	Conventional Hydrogen Bonds
	Asn142	3.65101	Hydrogen carbon bonds
Other	Met49	5.13551	Pi-Sulfur
Other	Cys145	4.13593	Pi-Sulfur
Hydrophobic	His41	4.79032	Pi-Alkyl

Table 3. 4WI ligand interactions on the docked 7TE0 protein

Category	Interaction	Bond distance (Å)	Bond type
Hydrogen bond	Cys145	3.6936	Conventional Hydrogen Bonds
	Glu166	2.04665	Conventional Hydrogen Bonds
	gln192	2.18163	Conventional Hydrogen Bonds
	Glu166	2.15552	Conventional Hydrogen Bonds
Halogen	Glu166	2.6779	Halogens (Fluorine)
	Arg188	3.47939	Halogens (Fluorine)
	Thr190	3.03429	Halogens (Fluorine)
Hydrophobic	His41	3.79223	Pi-Sigma
	Cys145	5.18576	Alkyl
	His163	4.60017	Pi-Alkyl

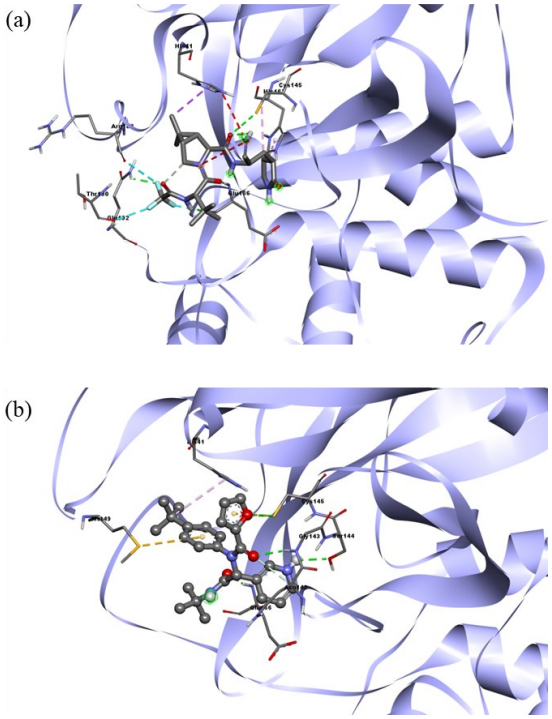

Figure 9. 3D interactions of a) 0EN-3V3M and b) 4WI-7TE0 complexes

3.3. Docking of Test Ligands

The test ligands used were derived from secondary metabolite compounds in 22 kinds of traditional Gorontalo medicinal plants. These plants include *Allium cepa* L., *Allium sativum*, *Jatropha curcas*, *Andrographis paniculata*, *Physalis angulata* L., *Carica papaya*, *Centella asiatica*, *Citrus hystrix*, *Curcuma longa*, *Euphorbia hirta*, *Musa balbisiana*, *Arcangelisia flava* L., *Trachyspermum roxburghianum*, *Syzygium aromaticum*, *Stachytarpheta jamaicensis*, *Strobilanthes cusia*, *Cinnamomum zeylanicum*, *Terminalia catappa*, *Zingiber officinale*, *Coriandrum sativum*, *Curcuma zedoaria*, and *Curcuma xanthorrhiza*. The active substance PF-07321332 from the paxlovid drug was also used in docking to obtain comparative data. A total of 830 test compounds underwent the docking process on each 3V3M and 7TE0 protein.

The test ligands were docked using Autodock Vina; therefore, the natural ligands previously docked using Autodock Tools were redocked using Autodock Vina. The results from the docking of natural ligands using Autodock Vina to determine the binding affinity value as an indicator in comparing receptor and ligand binding abilities as a SARS-CoV-2 inhibitor agent are shown in Table 4.

Table 4. Results of natural ligand redocking using Autodock Vina

Protein name	Natural ligand code	Mode	Affinity bindings (kcal/mol)	RMSD
Wuhan	0EN	1	-7.5	0.000
Omicron	4WI	1	-8.6	0.000

In the docking process of the test ligands, the grid boxes used were adjusted to the grid boxes validated by the docking method. Molecular docking can forecast the

interactions, conformations, and binding energies of proteins and their ligands. The identical grid box was utilized to maximize the formation of ligand bonds on the target protein's active site. The results of the best test ligand docking can be seen in Table 5.

Based on the binding affinity of the docking results, the compound physalin F from the *Physalis angulate* L. plant has the potential for inhibition of 3V3M protein with a binding affinity value of -10.3 kcal/mol. The physalin J compound from the *Physalis angulate* L. plant had the best inhibitory potential for the 7TE0 protein, whereas it had a binding affinity value of -8.9 kcal/mol. Figure 10 provides the most accurate two-dimensional representation of the interactions between complexes of amino acids and ligands.

Whereas for paxlovid, the results of docking and visualization of complex amino acid interactions in the 3V3M and 7TE0 proteins can be seen in Table 6 and Figure 11.

Table 5. The best docking results on 3V3M and 7TE0 proteins

Protein code	Ligand test	Binding affinity (kcal/mol)	Plant
3V3M	Physalin F	-10.3	*Physalis angulate* L.
	Physalin J	-10.2	*Physalis angulate* L.
	Physalin U	-10.2	*Physalis angulate* L.
	Physalin B	-9.5	*Physalis angulate* L.
	Physalin G	-9.1	*Physalis angulate* L.
	Physalin T	-8.9	*Physalis angulate* L.
	Thalifendine	-8.9	*Arcangelisia flava* L.
	Cyanin	-8.7	*Allium cepa* L.
	(+)-Homoaromoline	-8.6	*Arcangelisia flava* L.
	Physalin D	-8.5	-
	Limacine	-8.4	*Arcangelisia flava* L.
	Physalin I	-8.4	
	5-Carboxypyranocyanidin-3-O-beta-glucopyranoside	-8.3	*Allium cepa* L.
	Vitexin-2"-O-gallate	-8.3	*Terminalia catappa*
	Withangulatin E	-8.3	*Physalis angulate* L.
	Cyanidin-3-(6"-malonyllaminaribioside)	-8.2	*Allium cepa* L.
	Dihydrowithanolide E	-8.2	*Physalis angulate* L.
	Quercetin	-8.2	*Allium cepa* L.
	5-Hydroxy-7,8-dimethoxyflavone-5-glucoside	-8.1	*Andrographis paniculata*
	Cyanidin-3-(3",6"-dimalonylglucoside)	-8.1	*Allium sativum*
	Cyanidin-3-(3"-malonylglucoside)	-8.1	*Allium sativum*
	Cyanidin-3-(6"-malonylglucoside)	-8.1	*Allium sativum*
	Skullcapflavone-1,2'-O-beta-D-glucopyranoside	-8.1	*Andrographis paniculata*
	Verbascoside	-8.1	*Strobilanthes cusia*
	Withangulatin A	-8.1	*Physalis angulate* L.
	Alpha Amyrine	-8.0	*Euphorbia hirta*
	Cyanidin-3-O-glucoside	-8.0	*Allium cepa* L. / *Allium sativum*
	Hydroxyanigorufone	-8.0	*Musa balbisiana*
	Neoandrographolide	-8.0	*Andrographis paniculata*
	Peonidin-3-arabinoside	-8.0	*Allium cepa* L.
	Shogasulfonic acid D	-8.0	*Zingiber officinale*
	Withangulatin I	-8.0	*Physalis angulate* L.
	5,2',3'-Trihydroxy-7,8-dimethoxyflavone-3'-glucoside	-7.9	*Andrographis paniculata*
	Andrographidin A	-7.9	*Andrographis paniculata*
	Campesterol	-7.9	*Syzygium aromaticum*
	Euphorbianin	-7.9	*Euphorbia hirta*
	14-Acetyl-3,19-isopropylideneandrographolide	-7.8	*Andrographis paniculata*
	14-Deoxy-11,14-didehydroandrographolide	-7.8	*Andrographis paniculata*
	Myricetin-3-neohesperidoside	-7.8	*Physalis angulate* L.
	Palmarumycin JC1	-7.8	*Jatropha curcas*

Protein code	Ligand test	Binding affinity (kcal/mol)	Plant
	Palmarumycin JC2	-7.8	*Jatropha curcas*
	Paxlovid	-7.8	-
	Physagulin M	-7.8	*Physalis angulate* L.
	Physalin W	-7.8	*Physalis angulate* L.
	Quercetin-3-O-rhamnosyl-1-6-galactoside	-7.8	*Physalis angulate* L.
	Tellimagrandin I	-7.8	*Syzygium aromaticum*
	Chlorogenic acid	-7.7	*Andrographis paniculata and Stachytarpheta jamaicensis*
	Cyanidin-3-laminaribioside	-7.7	*Allium cepa* L.
	Gibberellin A1	-7.7	*Allium cepa* L. *dan pepaya*
	Gibberellin A4	-7,7	*Allium cepa* L.
	Shogasulfonic acid C	-7.7	*Zingiber officinale*
	Withaphysalin A	-7.7	*Physalis angulate* L.
	Andropanolide	-7.6	*Andrographis paniculata*
	Gibberellin A3	-7.6	*Carica papaya*
	Irenolone	-7.6	*Musa balbisiana*
	isoandrographolide	-7.6	*Andrographis paniculata*
	Kaempferol-4'-glucoside	-7.6	*Allium cepa* L
	Rutin	-7.6	*Euphorbia hirta*
7TE0	Physalin J	-8.9	*Physalis angulate* L
	Vitexin 2”-O-gallate	-8.8	*Terminalia catappa*
	Skullcapflavone 1,2'-O-beta-D-glucopyranoside	-8.8	*Andrographis paniculata*
	5-Carboxypyranocyanidin 3-O-beta-glucopyranoside	-8.7	*Allium cepa* L
	Paxlovid	-8.7	-
	Physalin F	-8.7	*Physalis angulate* L
	Cyanin	-8.6	*Allium cepa* L
	Physalin T	-8.6	*Physalis angulate* L
	Rutin	-8.6	*Euphorbia hirta*

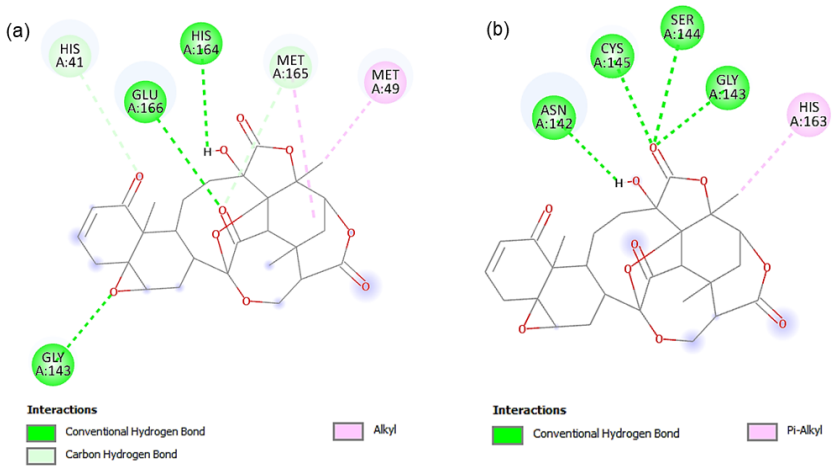

Figure 10. Interactions of the protein complex a) physalin F-3V3M, b) physalin J-7TE0

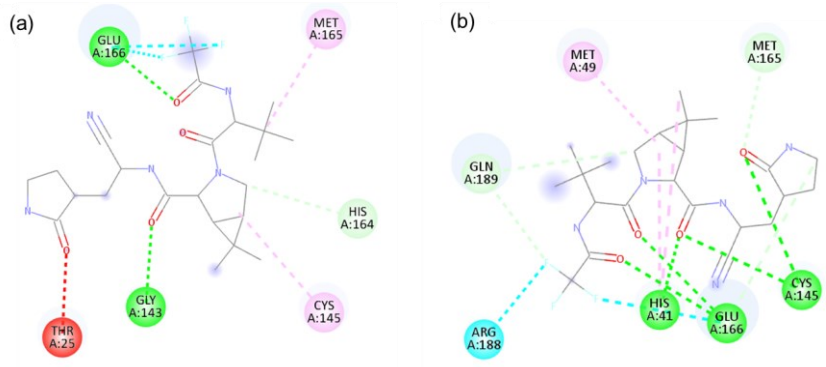

Figure 11. Interaction of the protein complex resulting from the docking of paxlovid ligands in the (a) Mpro Wuhan complex and (b) Mpro omicron

Table 6. Paxlovid docking results on 3V3M and 7TE0 proteins

Compound	Protein code	affinity bindings	RMSD
Paxlovid	3V3M	-7.8	0.000
	7TE0	-8.7	0.000

3.4. Molecular Dynamics

Protein topologies and ligands were produced separately in different orders. The protein topology was created using the pdb2gmx command. The force field used in protein topology was AMBER99SB-ILDN protein and nuclear AMBER94. This force field was chosen because it has improved simulation accuracy from the ff99SB force field [31]. The TIP3P water model was selected in this simulation. Meanwhile, the ligand topology was produced using the acpype program. Then a complex file was formed from the protein and ligand coordinate data.

The box area on the system was formed with the triclinic model with the editconf command. The solvent was added after the previously defined box was accompanied by adding Na and Cl ions to change the system to a neutral state [32]. The system must first minimize energy to achieve stability using the steepest descent method before entering Molecular dynamic production. Temperature and pressure were also regulated according to the simulation needs. In the 3V3M complex, the potential energy produced is around -4.6×10^5 kJ/mol. Whereas in the 7TE0 complex, the final energy yield of the system shows -4.7×10^5 kJ/mol. Convergent and declining graphs and system energy below -1×10^5 kJ/mol indicate that the minimization process has been successful.

The temperature parameter setting was done in the NVT phase of 50,000 steps. The system temperature was maintained using a modified Berendsen thermostat V-rescale at 300 K. Fluctuations occur in each ligand at different simulation time intervals. The highest fluctuations occurred in physalin J ligands at 50-60 ps and physalin F at 80-90 ps. Fluctuations appeared in the paxlovid ligand of the 7TE0 complex at 20-30 ps during the simulation. However, all ligands experience stability towards the end of the simulation. The system pressure was also regulated at the NPT equilibration stage. The system pressure was set at 1 bar using the Parrinello-Rahman barostat method.

After the energy, temperature, and pressure of the system are at optimal conditions, the next stage is the production of MD. MD production was conducted in 50,000,000 steps within 50 ns. The Grompp and mdrun commands are utilized to run this step. The integrated timestep was set at 2 fs, and the coordinates, output control energy, and log files were stored every 10 ps. Before analyzing the results of MD manufacturing, any atom damage was repaired by recentering and rewrapping coordinates. The performed analysis included RMSD, RMSF, and MMGBSA analysis.

During the simulation, the RMSD of the 3V3M and 7TE0 complexes were analyzed to determine the ligand bond stability on the protein's active site. RMSD size of less than 0.25 nm is acceptable and has similarities with the reference structure [33]. Increasing the plot of the RMSD results indicates increased ligand activity in finding the best binding site to the protein. When RMSD begins to show stability, the bonds formed by the ligands on the protein's active site tend to be maintained by the system [32]. The RMSD graph of the 3V3M complex is shown in Figure 12. With an average RMSD value of 0.18 nm, the physalin J ligand demonstrated the highest level of stability. Figure 13 depicts fluctuations in the 7TE0 complex; each test ligand also experiences fluctuations. The 7TE0-physalin J complex formed the stable RMSD graph for 50 ns, with an average thickness of 0.22 nm.

RMSF (root mean square fluctuation) analysis shows the flexibility of amino acids during the simulation. Sharp fluctuations describe the increased flexibility of amino acids, while low RMSF values indicate the limitations of movement experienced by amino acid residues [34]. The results of the RMSF analysis can be seen in Figure 14.

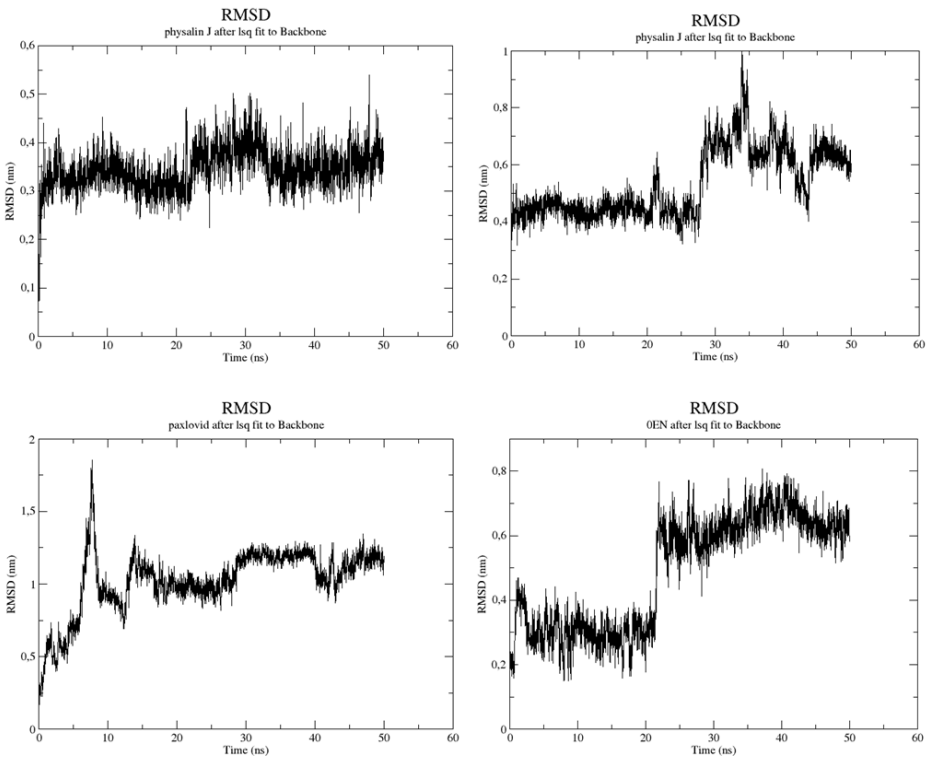

Figure 12. RMSD analysis of the 3V3M complex

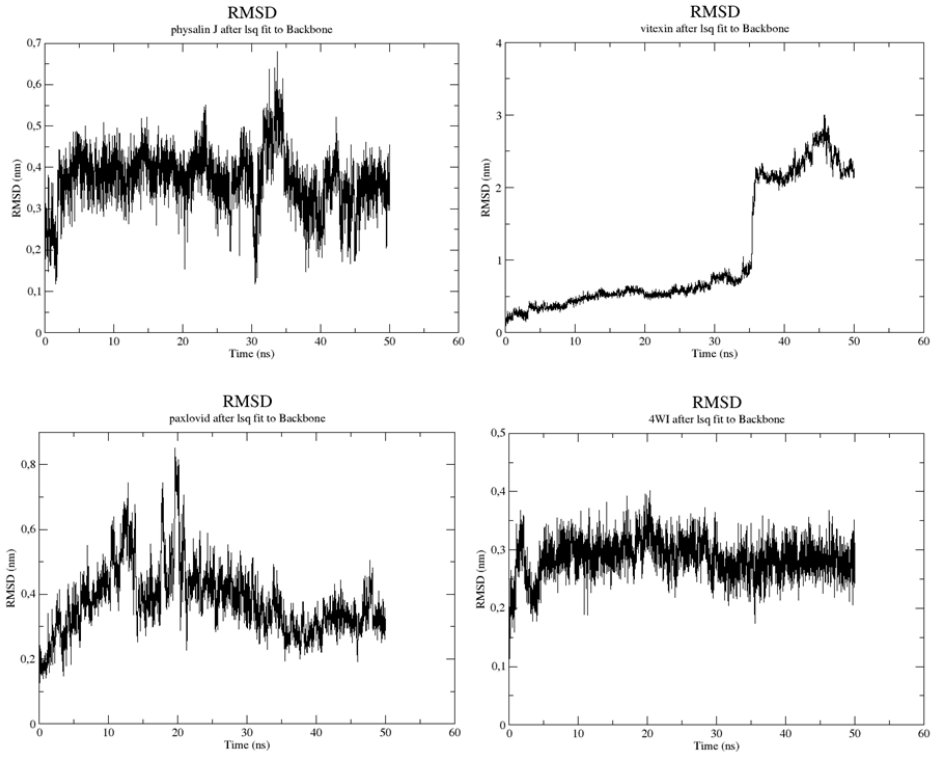

Figure 13. RMSD analysis of the 7TE0 complex

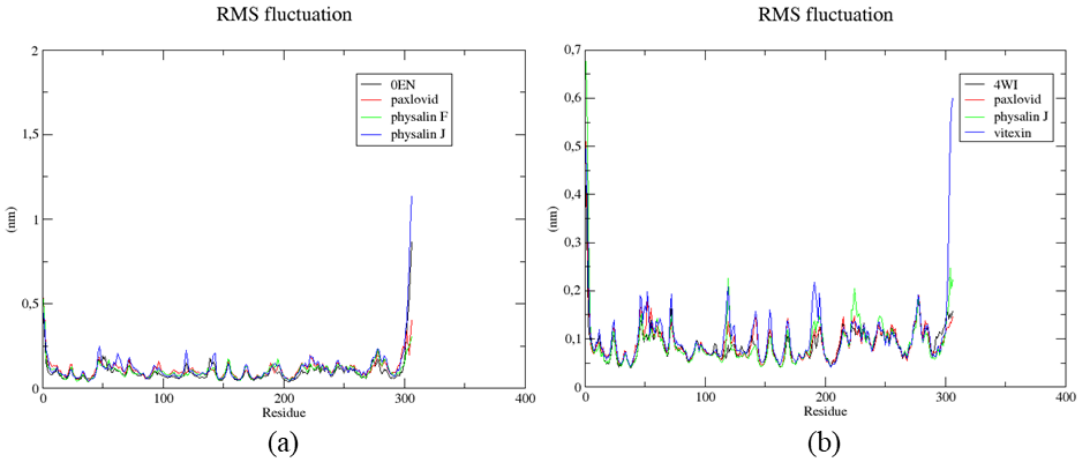

Figure 14. Complex RMSF results in a) 3V3M b) 7TE0

3.5. Molecular Mechanics Generalized Born Surface Area (MMGBSA)

In molecular dynamics simulations, the MMGBSA (Molecular Mechanics Generalized Born Surface Area) method is utilized to calculate the free energy of ligand-macromolecule bonds. Calculating bond-free energy values was used to predict the strength of the bonds formed [35]. Bond-free energy (ΔG), which has a negative value (≤ 0), goes straight with bonding ability. The more negative the result of ΔG, the stronger the bond formed.

Table 7. The results of the calculation of the bond-free energy MMGBSA method

Complex	ΔVDWAALS	ΔEEL	ΔEGB	ΔESURF	ΔGGAS	ΔGSOLV	ΔTOTAL
3V3M-0EN	-37.44	-13.24	28.68	-4.53	-50.67	24.15	-26.53
3V3M-paxlovid	-27.72	-14.54	26.37	-3.50	-42.25	22.87	-19.38
3V3M-physalin F	-36.61	-13.02	25.58	-4.17	-49.63	21.41	-28.22
3V3M-physalin J	-37.30	-13.79	28.64	-4.16	-51.08	24.47	-26.61
7TE0-4WI	-49.78	-48.78	57.70	-6.29	-98.56	51.40	-47.16
7TE0-paxlovid	-37.45	-11.46	28.19	-4.72	-48.92	23.47	-25.44
7TE0-physalin J	-38.50	-20.36	36.35	-4.11	-58.86	32.24	-26.62
7TE0-vitexin	-35.93	-30.42	43.43	-5.16	-66.35	38.27	-28.08

In the 3V3M complex, the ΔG values of the 0EN, paxlovid, physalin F, and physalin J ligand complexes were -26.53 kcal/mol, -19.38 kcal/mol, -28.22 kcal/mol, and -26.61 kcal/mol, respectively. In the 7TE0 complex that binds to the 4WI ligand, paxlovid, physalin J, and vitexin-2"-O-gallate show ΔG values of -47.16 kcal/mol, -25.44 kcal/mol, -26.62 respectively kcal/mol and -28.08 kcal/mol. Complete information about the energy produced in the MMGBSA analysis can be seen in Table 7.

4. Conclusion

Secondary metabolite compounds contained in Gorontalo traditional medicinal plants have the potential to be inhibitors of the main protease of SARS-CoV-2. Based on the binding affinity results from molecular docking and molecular dynamic simulations, *Physalis angulate* L. plants with the active compounds of physalin F and physalin J on the 3V3M protein and physalin J and Vitexin 2"-O-gallate on the *Terminalia catappa* plant for the 7TE0 protein have great potential as inhibitors. However, in terms of structural stability and active residues which play a role in binding, the compounds physalin F, physalin J, and Vitexin 2"-O-gallate did not show better results than the active substances in paxlovid.

Acknowledgment

The authors would like to thank the computational chemistry laboratory at Universitas Negeri Gorontalo for facilitating researchers in the research process.

References

[1] Muhammad Adnan Shereen, Suliman Khan, Abeer Kazmi, Nadia Bashir, Rabeea Siddique, COVID-19 infection: Emergence, transmission, and characteristics of human coronaviruses, *Journal of Advanced Research*, 24, (2020), 91-98 https://doi.org/10.1016/j.jare.2020.03.005

[2] Zheng Gong, Jun-Wei Zhu, Cui-Ping Li, Shuai Jiang, Li-Na Ma, Bi-Xia Tang, Dong Zou, Mei-Li Chen, Yu-Bin Sun, Shu-Hui Song, Zhang Zhang, Jing-Fa Xiao, Xue. Yong-Biao, Bao. Yi-Ming, Zheng-Lin Du, Wen-Ming Zhao, An online coronavirus analysis platform from the National Genomics Data Center, *Zoological Research*, 41, 6, (2020), 705 https://doi.org/10.24272/j.issn.2095-8137.2020.065

[3] Md. Rayhan Chowdhury, Md. Atik Mas-Ud, Md. Roushan Ali, Mst. Fatamatuzzohora, Ajmeri Sultana Shimu, Md. Anamul Haq, Md. Ashikul Islam, Md. Firose Hossain, Md. Hosenuzzaman, Md. Mominul Islam, Harmful effects of COVID-19 on major human body organs: a review, *Journal of Pure and Applied Microbiology*, 15, 2, (2021), 500-511 https://doi.org/10.22207/JPAM.15.2.14

[4] Devendra Saran, Parminder Kaur, Arshida Khatun, How does COVID-19 invade the human body, *The Science World*, 1, 2, (2021), 4-9

[5] Ifat Hanifah, Dody Riswanto, Siti Nurbani, The Impact of The Covid-19 Pandemic on The Economic, Social, Cultural, And Employment of Indonesian Civil Society, *Journal of Advanced Research in Dynamical and Control Systems*, 12, 2, (2020), 3112-3117 https://doi.org/10.5373/JARDCS/V12I2/S20201430

[6] Imrana Qadeer, K. B. Saxena, P. M. Arathi, *Universalising Healthcare in India: From Care to Coverage*, 1 ed., Springer Singapore, 2021, ^https://doi.org/10.1007/978-981-16-5872-3

[7] Linlin Zhang, Daizong Lin, Xinyuanyuan Sun, Ute Curth, Christian Drosten, Lucie Sauerhering, Stephan Becker, Katharina Rox, Rolf Hilgenfeld, Crystal structure of SARS-CoV-2 main protease provides a basis for design of improved α -ketoamide inhibitors, *Science*, 368, 6489, (2020), 409-412 https://doi.org/10.1126/science.abb3405

[8] Wen Cui, Kailin Yang, Haitao Yang, Recent progress in the drug development targeting SARS-CoV-2 main protease as treatment for COVID-19, *Frontiers in Molecular Biosciences*, 7, (2020), 616341 https://doi.org/10.3389/fmolb.2020.616341

[9] Shamaila Kausar, Fahad Said Khan, Muhammad Ishaq Mujeeb Ur Rehman, Muhammad Akram, Muhammad Riaz, Ghulam Rasool, Abdul Hamid Khan, Iqra Saleem, Saba Shamim, Arif Malik, A review: Mechanism of action of antiviral drugs, *International Journal of Immunopathology and Pharmacology*, 35, (2021), 1-12 https://doi.org/10.1177/20587384211002621

[10] Jennifer Couzin-Frankel, in: Science, American Association for the Advancement of Science, 2021, https://doi.org/10.1126/science.acx9605

[11] Io Antonopoulou, Eleftheria Sapountzaki, Ulrika Rova, Paul Christakopoulos, Inhibition of the main protease of SARS-CoV-2 (M^{pro}) by repurposing/designing drug-like substances and utilizing nature's toolbox of bioactive compounds, *Computational and Structural Biotechnology Journal*, 20, (2022), 1306-1344 https://doi.org/10.1016/j.csbj.2022.03.009

[12] Bethany Halford, in: Chemical & Engineering News, American Chemical Society, 2022

[13] Wen Wen, Chen Chen, Jiake Tang, Chunyi Wang, Mengyun Zhou, Yongran Cheng, Xiang Zhou, Qi Wu, Xingwei Zhang, Zhanhui Feng, Mingwei Wang, Qin Mao, Efficacy and safety of three new oral antiviral treatment (molnupiravir, fluvoxamine and Paxlovid) for COVID-1: a meta-analysis, *Annals of Medicine*, 54, 1, (2022), 516-523 https://doi.org/10.1080/07853890.2022.2034936

[14] Firtyane Lihawa, Ramli Utina, Wirnangsi Uno, Malonda Maksud, *Riset khusus eksplorasi pengetahuan lokal etnomedisin dan tumbuhan obat di indonesia berbasis komunitas*, Universitas Negeri Gorontalo, Gorontalo, 2012

[15] Yulia Vera, Susi Yanti, Penyuluhan Pemanfaatan Tanaman Obat dan Obat Tradisional Indonesia Untuk Pencegahan dan Penanggulangan Penyakit Hipertensi di Desa Salam Bue, *Jurnal Education and Development*, 8, 1, (2020), 11-14

[16] Novri Y. Kandowangko, *Kajian Etnobotani Tanaman Obat oleh Masyarakat Kabupaten Bonebolango Provinsi Gorontalo*, Gorontalo State University, Gorontalo, 2014

[17] Garrett M. Morris, Ruth Huey, William Lindstrom, Michel F. Sanner, Richard K. Belew, David S. Goodsell, Arthur J. Olson, AutoDock4 and AutoDockTools4: Automated docking with selective receptor flexibility, *Journal of Computational Chemistry*, 30, 16, (2009), 2785-2791 https://doi.org/10.1002/jcc.21256

[18] Oleg Trott, Arthur J. Olson, AutoDock Vina: improving the speed and accuracy of docking with a new scoring function, efficient optimization, and multithreading, *Journal of Computational Chemistry*, 31, 2, (2010), 455-461 https://doi.org/10.1002/jcc.21334

[19] Dassault Systemes Biovia, BIOVIA discovery studio, in: *Dassault Systèmes*, 2020

[20] A. Orin, R. Johnston, J. Clear, B. Skwarecki, Behind The App: The Story of Notepad++, *Lifehacker Australia*, 18, (2015)

[21] Demian Riccardi, Jerry M. Parks, Alexander Johs, Jeremy C. Smith, HackaMol: An Object-Oriented Modern Perl Library for Molecular Hacking on Multiple Scales, *Journal of Chemical Information and Modeling*, 55, 4, (2015), 721-726 https://doi.org/10.1021/ci500359e

[22] Noel M. O'Boyle, Michael Banck, Craig A. James, Chris Morley, Tim Vandermeersch, Geoffrey R. Hutchison, Open Babel: An open chemical toolbox, *Journal of Cheminformatics*, 3, 1, (2011), 1-14 https://doi.org/10.1186/1758-2946-3-33

[23] L. L. C. Schrödinger, The PyMOL molecular graphics system, version 1.8, in: *Schrödinger, L. L. C.*, 2015

[24] Mark James Abraham, Teemu Murtola, Roland Schulz, Szilárd Páll, Jeremy C. Smith, Berk Hess, Erik Lindahl, GROMACS: High performance molecular simulations through multi-level parallelism from laptops to supercomputers, *SoftwareX*, 1, (2015), 19-25 https://doi.org/10.1016/j.softx.2015.06.001

[25] P. J. Turner, XMGRACE, Version 5.1. 19, in: *Center for Coastal and Land-Margin Research, Oregon Graduate Institute of Science and Technology, Beaverton, OR*, 2005

[26] Shuhui Song, Lina Ma, Dong Zou, Dongmei Tian, Cuiping Li, Junwei Zhu, Meili Chen, Anke Wang, Yingke Ma, Mengwei Li, Xufei Teng, Ying Cui, Guangya Duan, Mochen Zhang, Tong Jin, Chengmin Shi, Zhenglin Du, Yadong Zhang, Chuandong Liu, Rujiao Li, Jingyao Zeng, Lili Hao, Shuai Jiang, Hua Chen, Dali Han, Jingfa Xiao, Zhang Zhang, Wenming Zhao, Yongbiao Xue, Yiming Bao, The global landscape of SARS-CoV-2 genomes, variants, and haplotypes in 2019nCoVR, *Genomics, Proteomics & Bioinformatics*, 18, 6, (2020), 749-759 https://doi.org/10.1016/j.gpb.2020.09.001

[27] Siqi Wu, Chang Tian, Panpan Liu, Dongjie Guo, Wei Zheng, Xiaoqiang Huang, Yang Zhang, Lijun Liu, Effects of SARS - CoV - 2 mutations on protein structures and intraviral protein–protein interactions, *Journal of Medical Virology*, 93, 4, (2020), 2132-2140 https://doi.org/10.1002/jmv.26597

[28] María J. R. Yunta, How important is to account for water when modeling biomolecular complexes, *American Journal of Modeling and Optimization*, 3, 3, (2015), 68-86

[29] G. Madhavi Sastry, Matvey Adzhigirey, Tyler Day, Ramakrishna Annabhimoju, Woody Sherman, Protein and ligand preparation: parameters, protocols, and influence on virtual screening enrichments, *Journal of Computer-Aided Molecular Design*, 27, 3, (2013), 221-234 https://doi.org/10.1007/s10822-013-9644-8

[30] Neni Frimayanti, Musyirna Rahmah Nasution, Elsa Etavianti, Molecular docking and molecular dynamic simulation of 1, 5-benzothiazepine chalcone derivative compounds as potential inhibitors for Zika virus helicase, *Jurnal Riset Kimia*, 12, 1, (2021), 44-52 https://doi.org/10.25077/jrk.v12i1.365

[31] Kresten Lindorff - Larsen, Stefano Piana, Kim Palmo, Paul Maragakis, John L. Klepeis, Ron O. Dror, David E. Shaw, Improved side - chain torsion potentials for the Amber ff99SB protein force field, *Proteins: Structure, Function, and Bioinformatics*, 78, 8, (2010), 1950-1958 https://doi.org/10.1002/prot.22711

[32] Fauzan Zein Muttaqin, Halim Ismail, Hubbi Nasrullah Muhammad, Studi molecular docking, molecular dynamic, dan prediksi toksisitas senyawa turunan alkaloid naftiridin sebagai inhibitor protein kasein kinase 2-A pada kanker leukemia, *Pharmacoscript*, 2, 1, (2019), 49-64

[33] P. G. Bolhuis, Sampling kinetic protein folding pathways using all-atom models, in: *Computer Simulations in Condensed Matter Systems: From Materials to Chemical Biology Volume 1*, Springer, 2006, https://doi.org/10.1007/3-540-35273-2_11

[34] Priyashi Rao, Arpit Shukla, Paritosh Parmar, Rakesh M. Rawal, Baldev Patel, Meenu Saraf, Dweipayan Goswami, Reckoning a fungal metabolite, Pyranonigrin A as a potential Main protease (M^{pro}) inhibitor of novel SARS-CoV-2 virus identified using docking and molecular dynamics simulation, *Biophysical Chemistry*, 264, 106425, (2020), 1-11 https://doi.org/10.1016/j.bpc.2020.106425

[35] Frithjof Godschalk, Samuel Genheden, Pär Söderhjelm, Ulf Ryde, Comparison of MM/GBSA calculations based on explicit and implicit solvent simulations, *Physical Chemistry Chemical Physics*, 15, 20, (2013), 7731-7739 https://doi.org/10.1039/C3CP00116D